

Effects of Confinement in Carbon Nanotubes on the Performance and Lifetime of Fischer-Tropsch Iron Nano Catalysts

*Tavasoli, Ahmad**⁺

Faculty of Chemistry, University of Tehran, Tehran, I.R. IRAN

Anahid, Sanaz; Nakhaeipour, Ali

Research Institute of Petroleum Industry, Tehran, I.R. IRAN

ABSTRACT: *The effects of confinement in carbon nanotubes on Fischer-Tropsch (FT) activity, selectivity and lifetime of Carbon NanoTubes (CNTs) supported iron catalysts are reported. A method was developed to control the position of the catalytic sites on either inner or outer surface of carbon nanotubes. TEM analyses revealed that more than 80% of iron oxide particles can be controlled to be positioned at inner or outer surface of the nanotubes. Deposition of iron oxide inside the nanotube pores decreased the average size of the iron oxide particles from 14 to 7nm and shifted the reduction peak temperature of iron oxide species to lower temperatures (from 389 to 371°C, 428 to 413°C and 580 to 530°C) and improved the reducibility of the catalyst by 25%. Catalytic performances of the catalysts in terms of FT experiment were tested in a fixed-bed micro reactor; the catalyst with catalytic sites inside the pores showed 23% higher initial activity than the catalyst with catalytic sites outside the pores. Also, the catalyst with catalytic sites inside the pores exhibited higher selectivity to heavier hydrocarbons (40.5% vs. 32.9% C₅⁺ selectivity). In addition, deposition of catalytic sites on interior surface of the nanotubes resulted in a more stable catalyst, while its counterpart experienced 46.4% deactivation within a period of 720 h due to catalytic sites sintering. It is concluded that encapsulation of the catalytic nanoparticles inside the nanotubes prevents the catalytic site agglomeration.*

KEY WORDS: *Fischer-Tropsch, Iron nano particles, Carbon nanotubes, Confinement, Activity, Selectivity, Deactivation.*

INTRODUCTION

The Fischer-Tropsch (FT) synthesis offers the possibility of converting a mixture of hydrogen and carbon monoxide (synthesis gas) into clean hydrocarbons, free of sulfur [1-3]. FT process is a surface polymerization

reaction which can be catalyzed by iron, cobalt and ruthenium at pressures from 1-6 MPa and temperatures from 200 to 300 °C [3]. Supported and unsupported iron catalysts have been studied for the conversion of syngas,

* To whom correspondence should be addressed.

+ E-mail: tavassolia@khayam.ut.ac.ir

1021-9986/10/3/1

13/\$/3.30

obtained from biomass, coal and natural gas [4,5]. In order to achieve high surface active sites, iron precursors are dispersed on porous carriers; with silica, alumina and titania being the most frequently used. A drawback of these support materials is their reactivity toward active metal, which during preparation or catalysis results in the formation of mixed compounds that are reducible only at high reduction temperatures. Recently, other supports such as carbon in the form of activated carbon and carbon nanotubes (CNTs) have been used in the FT reactions [6-13]. Carbon nanotubes (CNTs) have many unique properties such as superior electronic conductivity and high capacity of hydrogen uptake, and are attracting increasing attention as novel support media for heterogeneous catalysis. For chemical reactions influenced by an electronic factor, the electronic conductivity of the supports is important. The main advantage of using CNTs as support materials for catalysis is that they possess both high surface area and good electronic conductivity in comparison with the conventional carbon materials, such as graphite (low surface area) and activated carbon (poor electronic conductivity).

There are some studies on the application of CNTs as support for Co and/or Fe catalysts [6-7, 10-13]. However controversy encircled the stability of CNTs supported FT catalysts. Bahome, et al [11,13] studied Fe based catalysts supported on carbon nanotubes for use in the FT reaction which were prepared either by incipient wetness or a deposition precipitation method. They have reported that Fe/CNTs catalyst is an active and stable catalyst. However, van Steen & Prinsloo [12] observed a rapid deactivation for Fe/CNTs catalyst in FTS. Catalyst stability is an important performance variable in iron catalyzed FTS processes. The deactivation behavior of iron catalysts is mainly due to the following reasons: oxidation, metal migration into the support lattice resulting in the formation of the inactive FT compounds, the aggregation and growth of metal iron on the surface of the catalyst and the loss of metal iron because of attrition (especially for the three-phase slurry bed reactor) [5].

In our previous work, we extensively studied the activity and product selectivity of CNTs supported iron catalysts [5]. In the present work, we intend to enhance the activity, selectivity and lifetime of the CNTs supported iron catalyst by confinement of iron within the CNTs. We introduced the iron species into the channels

of CNTs. The FT activity and selectivity of this new catalyst have been studied for a long time (i.e. 720 h) and the results were compared to those of the catalyst with iron nanoparticles dispersed mostly on the outer walls of the CNTs.

EXPERIMENTAL SECTION

Catalyst preparation

Multiwall carbon nano tubes (MWCNTs) (purity >95%) was used as support material for the preparation of iron FT synthesis catalysts. The CNTs were first treated in nitric acid aqueous solution as follows. 10 g of CNT samples were suspended in 500 ml of 68wt.% HNO₃ and refluxed at 140°C for 16 hours. The mixture was cooled down to room temperature, filtered and washed with deionized water until the pH value of the filtrate reached around 7. Then the CNTs were dried at 120°C for 12 h. For the preparation of the catalyst with 10 wt% Fe, 3.2 g Fe(NO₃)₃·9H₂O was dissolved into deionised water. The treated nanotubes were added into the aqueous solution under stirring followed by ultrasonic treatment and simultaneous stirring for 2 h. Then the solvent was gradually dried at 140°C in air for 4 h. Finally, the catalyst was calcined at 350°C for 3 hours. The sample is denoted as Fe.in/CNT. For comparison, the same amount of iron was deposited on the surface of raw nanotubes by impregnating untreated CNTs with aqueous Fe(NO₃)₃·9H₂O solution. After impregnation, the same drying and calcination procedure was applied and Fe.out/CNTs was obtained.

Inductivity coupled plasma (ICP)

The iron loadings of supports and the calcined fresh and used catalysts were verified by Inductivity Coupled Plasma (ICP) AES system.

Transmission Electron Microscopy (TEM)

The CNTs, calcined fresh and used catalysts were characterized by Transmission Electron Microscopy (TEM). Sample specimens for TEM studies were prepared by ultrasonic dispersion of the CNTs and catalysts in ethanol. The suspensions were dropped onto a carbon-coated copper grid. TEM investigations were carried out using a Hitachi H-7500 (120kV). Several TEM micrographs were recorded for each sample and analyzed to determine the particle size distribution.

BET surface area measurements / BJH pore size distributions

The surface area, pore volume, and average pore radius of the CNTs, calcined fresh and used catalysts were measured by an ASAP-2000 system from micromeritics. The samples were degassed at 200 °C for 2 h under 50 mTorr vacuum and their BET area, pore volume, and average pore radius were determined.

X-ray diffraction

XRD measurements of the CNTs, calcined fresh and used catalysts were conducted with a Philips PW1840 X-ray diffractometer with monochromatized Cu/K α radiation. The crystallite diameter was determined by substituting the half-width of a chosen peak into the Debye-Scherrer equation.

Temperature programmed reduction

Temperature programmed reduction (TPR) spectra of the calcined fresh and used catalysts were recorded using a CHEMBET-3000, equipped with a thermal conductivity detector. The catalyst samples were first purged in a flow of helium at 150°C, to remove traces of water, and then cooled to 40°C. The TPR of 100 mg of each sample was performed using 3.1% hydrogen in nitrogen gas mixture with a flow rate of 40 cm³/min. The samples were heated from 40 to 900 °C with a heating rate of 10 °C /min.

Reaction setup and experimental procedure

The Fischer-Tropsch synthesis was performed in a fixed-bed micro reactor. Prior to CO hydrogenation, in-situ reduction was conducted according to the following procedure. The catalyst (1g) was placed in the reactor and diluted with 7g silicon carbide and pure hydrogen was introduced at a flow rate of 30 mL/min. The reactor temperature was increased from room temperature to 380°C at a rate of 1°C/min and maintained at this activation conditions for 12 h. After the activation period, the reactor temperature was decreased to 275 °C under flowing hydrogen. Hydrogen and syngas flow rates were controlled by Brooks-5850 mass flow controllers. Argon was used as internal standard gas in the reactor feed. The mixed gases (30%CO, 60%H₂, 10% Ar) entered through to the top of the fixed bed reactor. The temperature of the reactor was controlled via a PID temperature controller. Synthesis gas with a flow rate of 45 mL/min (H₂/CO ratio of 2) was introduced and the reactor pressure was increased to

2 MPa. Products were continuously removed from the vapor and passed through two traps. The uncondensed vapor stream was reduced to atmospheric pressure. The composition of the outlet gas stream quantified using an on-line GC-2014 Shimadzu gas chromatograph. The contents of traps were removed every 24h, the hydrocarbon and water fractions separated, and then analyzed by a Varian 3400 GC. Catalytic activity, product selectivity and stability of catalyst were evaluated during reaction period of 720 hours.

The %CO conversion and FTS rate were calculated as:

$$\%CO = \frac{CO_{in} - CO_{out}}{CO_{in}} \quad (1)$$

$$FTS \text{ rate} = \frac{\text{g of hydrocarbons}}{\text{g of cat. h}} \quad (2)$$

The hydrocarbon product (C_i) selectivities S(C_i) were calculated as follows:

$$S(C_i) = \frac{\text{mass of component } C_i}{\sum C_i} \quad (3)$$

RESULTS AND DISCUSSION

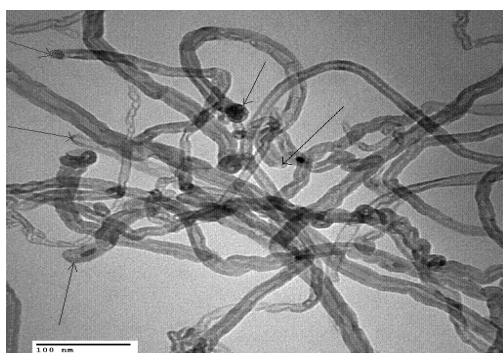
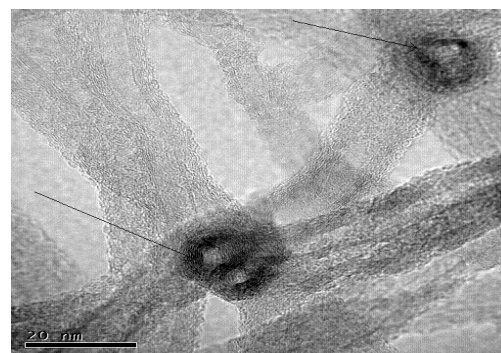
Characterization overview

Table 1 shows the metal content for the untreated fresh CNTs, acid treated CNTs, and the catalysts. ICP analysis revealed that the amount of encapsulated metal content in fresh CNTs was about 0.6wt% which decreased to zero for acid treated CNTs. Also Table 1 shows that the metal contents of the fresh catalysts were fairly similar and close to the target metal content of 10 wt%. In addition, the metal content of the used catalysts are very close to the fresh calcined catalysts indicating that 720 h FT synthesis did not change the metal content of the catalysts.

Samples of the untreated fresh CNTs and acid treated CNTs material were analyzed by TEM. Both samples were comprised of interwoven matrix of tubes (Figs. 1a, 1b & 2) that were shown to be comprised of multi-walled carbon nanotubes (MWCNTs). Fig. 1a shows that the untreated sample has uniform nanotubes and their inner and outer diameters vary between 5-12 nm and 10-25 nm, respectively. Fig. 1b shows a high resolution image of the fresh CNTs sample presenting graphite layers of multi-wall CNTs with closed caps. As can be seen in the case of untreated CNTs, residual metal particles were encapsulated in the nanotubes during the synthesis procedure and most of the nanotube caps are closed (Fig. 1a & 1b). In fact, these

Table 1: Characteristic (ICP and BET) of the supports and fresh and used catalysts.

Support/Catalyst	Residual Metal Content %	Targeted Metal Content%	Total Iron Content %	BET Surface Area (m ² /g)	Total Pore Volume (cm ³ /g)	Average Pore Diameter (nm)	Particle size (nm) different by XRD
Fresh CNTs	0.6	-	-	178	0.47	11.2	-
Treated CNTs	0	-	-	253.4	0.63	10.7	-
Fresh calcined Fe.out/CNTs	-	10	9.7	182	0.47	11.2	15
Fresh calcined Fe.in/CNTs	-	10	9.5	212	0.52	10.9	7.6
Used Fe.out/CNTs	-	10	9.5	179	0.47	11.2	39
Used Fe.in/CNTs	-	10	9.5	212	0.52	10.9	14.5

**Fig. 1a: TEM image of untreated fresh CNTs, some closed caps are shown by arrows.****Fig. 1b: A high resolution TEM image of the fresh CNTs sample presenting graphite layers of multi-wall CNTs with closed caps.**

metal particles are confined in the inner core of CNTs and blocked the pores. As shown in Fig. 2, refluxing of the CNTs in concentrated nitric acid opened the caps of the closed tubes, cut them into smaller segments and created some defects on the outer surface of the CNTs. In the case of untreated sample most of the nanotube caps are closed while the population of open-cap nanotubes increases with the acid treatments significantly. This is confirmed with the nitrogen adsorption analysis as untreated sample possess low surface area and low pore volume as a result of pore blockage (see Table 1). Treatment with acid increased the BET surface area of the CNTs by 42.5% (Table 1). At the same time the pore volume of the CNTs were increased from 0.47 to 0.63. For both samples, a simple calculation on the enhancement of surface area can give the ratio of open-cap CNTs to the closed caps before and after the acid treatments. Supposing the n_t , n_{op} and n_{cl} are the total number of nanotubes, the number of open cap, and the number of closed cap nanotubes per unit mass, respectively and L is the nanotubes average length.

The percentage of open-cap CNTs based on measured surface area (A) can be calculated as follows:

$$n_t = n_{cl} + n_{op} \quad (4)$$

$$A_{\text{untreated}} = n_t \cdot d_{\text{out}} \cdot \pi \cdot L \quad (5)$$

$$A_{\text{treated}} = n_{op} \cdot d_{\text{out}} \cdot \pi \cdot L + n_{op} \cdot d_{\text{in}} \cdot \pi \cdot L + n_{cl} \cdot d_{\text{out}} \cdot \pi \cdot L \quad (6)$$

$$\frac{A_{\text{untreated}}}{A_{\text{treated}}} = \frac{n_t \cdot d_{\text{out}}}{n_{op} \cdot d_{\text{out}} + n_{op} \cdot d_{\text{in}} + n_{cl} \cdot d_{\text{out}}} \quad (7)$$

Considering average $D_{\text{out}} = 20$ nm, $D_{\text{in}} = 10$ nm, $A_{\text{untreated}} = 178$ and $A_{\text{treated}} = 253.4$ m²/g:

$$\frac{n_{op}}{n_t} = 85\% \quad (8)$$

The calculation shows that more than 85 percent of closed-cap nanotubes became open-cap due to refluxing of the CNTs in concentrated nitric acid at 140°C.

Figs. 3 and 4 show the TEM of iron loaded Fe.out/CNTs and Fe.in/CNTs catalysts. Dark spots represent the iron

oxides which are attached inside or outside of the nanotubes. As shown, in the case of Fe.out/CNTs catalyst most of the doped metals are attached to the exterior layer of the CNTs. This is because most of their inner cores are blocked and aqueous solution can only wet the exterior surface. TEM analysis has shown that diameter of metal particles on the surface of this catalyst varies between 5-29 nm. However, in the case of Fe.in/CNTs catalyst the majority of the iron particles were distributed inside the tubes and the rest on the outer surface of the CNTs (more than 80%). This can be attributed to carbon nanotubes tubular morphology which can induce capillary forces during the impregnation process. In addition, the particles inside the tubes are fairly uniform and the most abundant ones are 3-9 nm in size (Fig. 4) in accordance with the average inner diameter of the CNTs, whereas those on the outer surface have grown to 17.6 nm (Fig. 4). It seems that the CNTs channels have restricted the growth of the particles inside the tubes. Two bar graphs depicting the size distribution of the particles which are taken using 10 TEM pictures are shown in Figs. 5 and 6 for the Fe.out/CNTs and Fe.in/CNTs catalysts, respectively. The average size of the particles for Fe.out/CNTs and Fe.in/CNTs catalysts are 14 and 7 nm, respectively.

Figs. 7 and 8 show TEM images of the used Fe.out/CNTs and Fe.in/CNTs catalysts. As shown, in the case of both catalysts, the iron oxide particles inside the channels do not experience particle agglomeration significantly. This phenomenon can be related to the interaction of the catalytic sites with the inner surface of the pores and perhaps to the spatial restriction of the CNT channels [14-17]. However, most of the iron species on the exterior surface are agglomerated, resulting in lower catalytic dispersion under FT reactions. For Fe.out/CNTs catalyst the particle size distribution shifted considerably toward larger particles with an average of 36 nm and maximum particle size of 73 nm. Also for Fe.in/CNTs catalyst, the particle size distribution shifted toward larger particles with an average of 14 nm and maximum particle size of 42.7 nm. It can be concluded that the deposition of the catalytic sites inside the nanotube pores results in relatively more stable catalyst than that deposited on exterior surface of the nanotubes. To study the changes in particle size distributions and mechanism for the catalytic site agglomeration, several TEM images from the used catalysts were taken and analyzed. The results are shown in Figs. 9 and 10. In order to

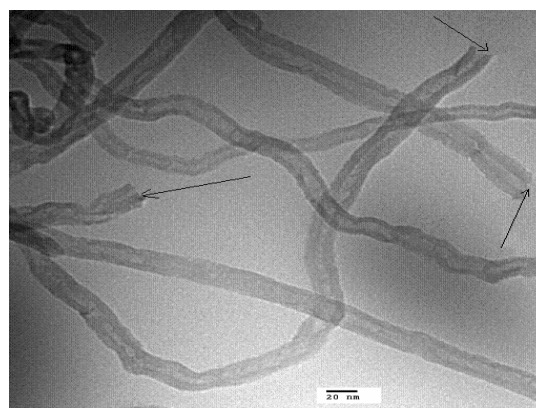


Fig. 2: TEM image of acid treated CNTs, some open caps are shown by arrows.

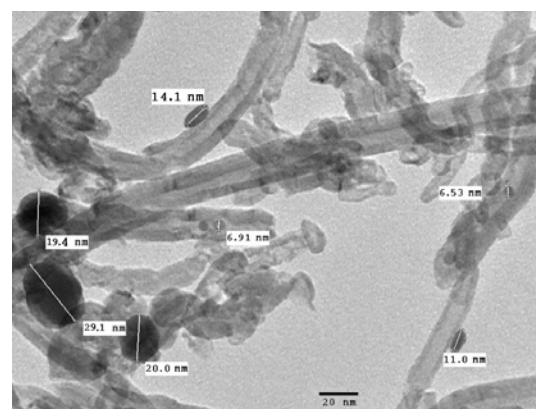


Fig. 3: The TEM of iron loaded fresh Fe.out/CNTs catalyst.

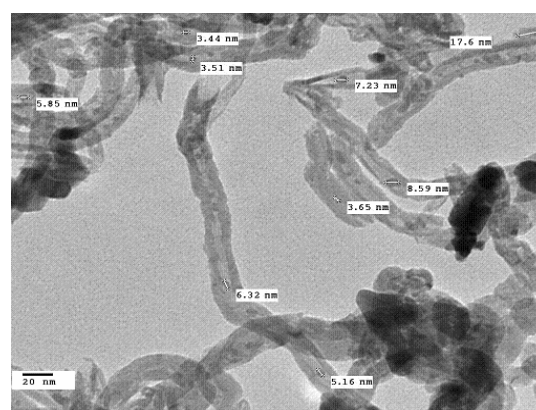


Fig. 4: The TEM of iron loaded fresh Fe.in/CNTs catalyst.

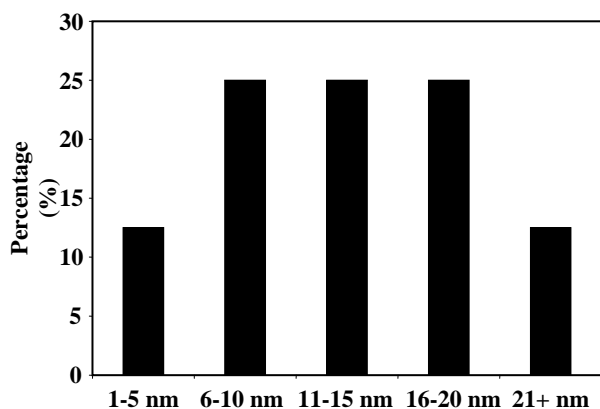


Fig. 5: Particles size distribution for the fresh Fe.out/CNTs catalyst.

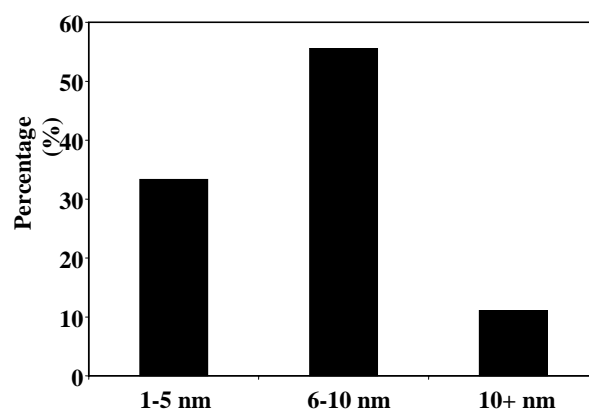


Fig. 6: Particles size distribution for the fresh Fe.in/CNTs catalyst.

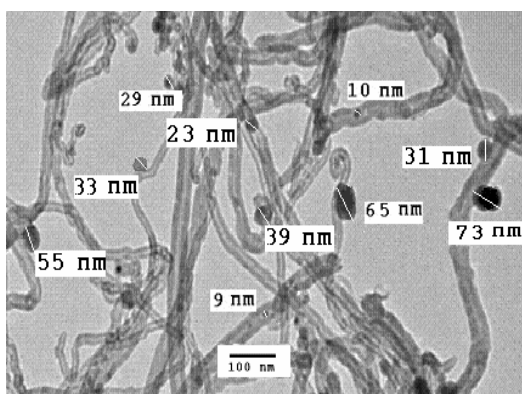


Fig. 7: The TEM of used Fe.out/CNTs catalyst.

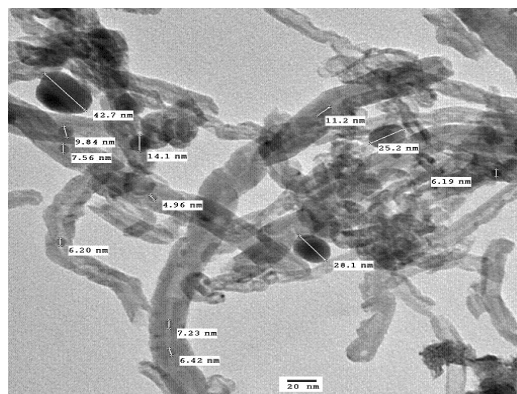


Fig. 8: The TEM of used Fe.in/CNTs catalyst.

describe the catalytic site agglomeration, two mechanisms namely, atom migration (Ostwald ripening) and crystallite migration (coalescence) are generally considered. According to the Ostwald ripening theory, metal atoms are released from one metal particle and attached to another metal particle. The difference in surface energy is the driving force for this process. In the case of the coalescence process, the movement of crystallites themselves over the support results in the particle collision and formation of larger particles. In both processes, sintering slows down with time resulting in a stable state [18]. In order to distinguish between these two models, the pattern of particle size distribution after sintering is generally studied. It has been shown that the Ostwald ripening results in a particle size distribution with a tail toward small particle sizes and a steep slope toward larger particle sizes [18,19]. As can be seen in Figs. 9 and 10, for both Fe.out/CNT and Fe.in/CNTs catalysts there is a Log-normal distribution with a tail toward small particle sizes. Thus, the Ostwald ripening can be

considered as the mechanism for metal site agglomeration for iron catalysts supported on the carbon nanotubes. Similar mechanism has been proposed for migration of transition metal over carbon base supports [20]. Results of nitrogen adsorption analysis for the catalysts are shown in Table 1. For the Fe.out/CNTs catalyst, the doped metal increased the surface area to some extent, however, there is no change in total pore volume. This is because the dispersed iron particles attach to the exterior layer of nanotubes and expand the surface area. For Fe.in/CNTs catalyst, the loading of 10% Fe decreased the surface area to 212 m²/g which indicates pore blockage due to iron loading on the support. Also the pore volume is decreased from 0.63 to 0.52 which can confirm the pore blockage of the treated CNTs.

Fig. 11 shows XRD patterns of calcined fresh Fe.out/CNTs and Fe.in/CNTs catalysts. Both of the catalysts show similar XRD patterns between 2 θ values of 10 and 50°. The diffraction peaks match very well with

the standard hematite phase. For both Fe.out/CNTs and Fe.in/CNTs catalysts the peaks at 2θ values of 26° and 43° correspond to graphite layers (multiwall carbon nanotubes), while the other peaks in the spectrum of catalysts are related to different crystal planes of Fe_2O_3 . The peak at 35.7° is the most intense peak of Fe_2O_3 in XRD spectrum of the Fe.out/CNTs and Fe.in/CNTs catalysts. Table 1 shows the average Fe_2O_3 particle size on the catalysts calculated from XRD spectrum and Debye-Scherrer equation at 35.7° . The average particle sizes decreased from 15 to 7.6 upon treatment of the support with nitric acid. There is a good agreement between the data for average particle size calculated based on XRD and TEM size distribution. The data reveal that the treatment of the CNTs with 68 wt.% nitric acid resulted in smaller crystalline sizes. As discussed earlier, this could be ascribed to the treatment which increases the surface area and also opens the caps on the closed CNTs, which in turn leads to higher surface area and better distribution of the metal particles and result in smaller iron cluster sizes. In addition the treatment with nitric acid provides more functional groups resulting in a higher dispersion and smaller particle sizes.

Fig. 12 shows XRD patterns of the used catalysts after 720 h of FTS reaction at 275°C . The diffraction peaks in the XRD of the used catalysts match very well with magnetite (Fe_3O_4) phase and the standard carbide Fe_5C_2 phase. However the particle size calculation based on XRD peak broadening reveals significant metal size growth for the used catalysts. As can be seen in the Table 1, in the case of Fe.out/CNTs, a sharp peak has appeared at 2θ value of 35.6° indicating considerable metal particle growth (i.e. from 15 nm to 39 nm) whereas, for the catalyst pretreated at strong acid environment, the metal particle growth is not significant compared to its counterpart (i.e. from 7.6 to 14.5 nm). As also shown by the TEM pictures, the iron particles which are inside the tubes did not enlarge as much as the iron particles located on the outer layer of the tubes. Lower interaction between the iron and the CNTs may be the main reason for the iron particles growth. The corresponding peaks for iron carbide phase (Fe_5C_2) appeared in the XRD spectra of the used Fe.in/CNTs catalyst at 2θ values of 39° and 41° while there was a small peak at 2θ value 41° in XRD of the used Fe.out/CNTs catalyst for iron carbide phase. This evidence showed that for the Fe.in/CNTs catalyst, the iron carbide content was higher and more stable during the 720 h FT reactions.

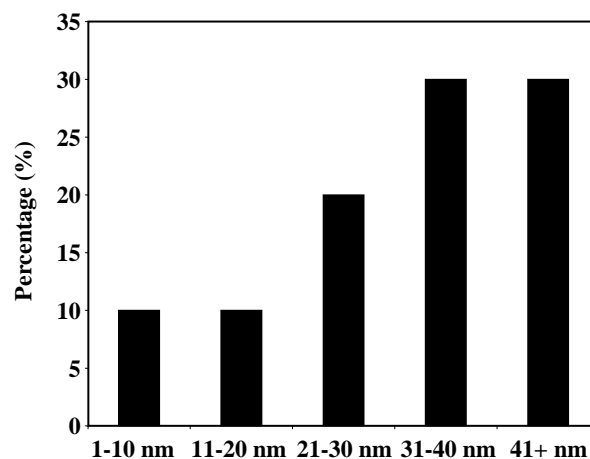


Fig. 9: Particles size distribution for the used Fe.out/CNTs catalyst.

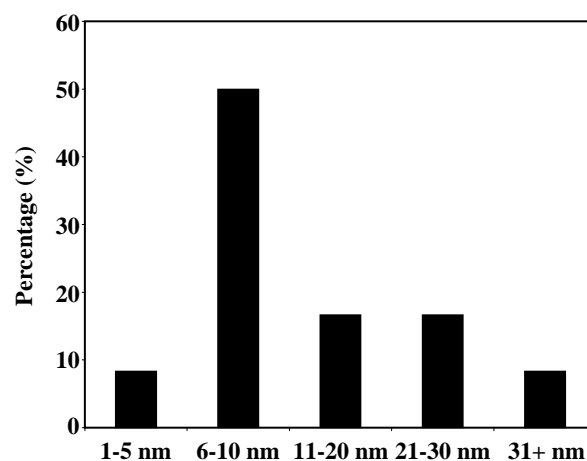


Fig. 10: Particles size distribution for the used Fe.in/CNTs catalyst.

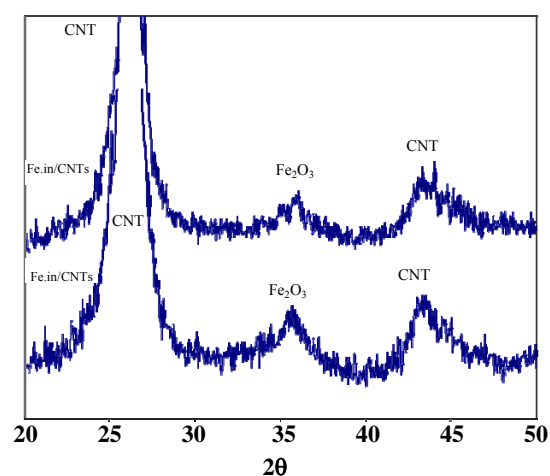


Fig. 11: XRD spectra for the fresh catalysts.

Temperature Programmed Reduction (TPR) is a powerful tool to study the reduction behavior of oxidized phases; in some cases it is also possible from the reduction profiles of supported oxides to obtain useful information about the degree of interaction of the active metal with the support. TPR patterns of the fresh and used Fe.out/CNTs and Fe.in/CNTs catalysts are shown in Figs. 13 and 14. Four peaks can be observed on the TPR profile of the fresh catalysts. Generally, the reduction of iron oxides takes place as below:



In the spectra of the fresh Fe.out/CNTs catalyst, the first peak observed at 389°C, could be assigned to the reduction of Fe_2O_3 to Fe_3O_4 . The second peak, observed at 428°C, could be assigned to the subsequent reduction of Fe_3O_4 to FeO. Third peak, observed at 580°C, could be related to the reduction of FeO to metallic Fe. And finally, the peak observed at 650°C corresponds to gasification of CNTs. Figs. 13 and 14 show reduction temperature for the fresh and used catalysts. According to the reduction peak temperatures shown in this table, deposition of iron oxide particles inside the nanotubes which caused a significant decrease in metal particle sizes (i.e. 7.6 nm in comparison with 14.5 nm) results in a decrease in the temperature of the first TPR peak from 389 to 371 °C and that of the second and third from TPR peaks from 428 to 413 °C and 580 to 530 °C, respectively. It has been shown that the confinement of iron oxides inside the CNTs pore resulted in smaller metal particle sizes and easier reduction at lower temperatures [14]. It can be concluded that iron oxide interacts with the interior CNTs wall differently from that with the exterior wall. It has been postulated that the electron deficiency of the interior CNTs surface is possibly responsible for this phenomenon [14-17]. Higher degree of reduction will make more iron atoms available for FTS reaction in the Fe.in/CNTs catalyst in comparison with Fe.out/CNTs catalyst.

More detailed values for the degree of reduction and the total amount of hydrogen consumptions during TPR are given in Table 2. The degree of reduction of the metal (DR_T) is the ratio of H_2 consumed during reduction from room temperature to 900°C to the calculated amount of H_2 for the complete reduction of metal oxides. For complete reduction of 10% iron catalyst, 2.67 mmol/g-cat is required. For both catalysts, the degrees of reduction were low despite the high temperature in the TPR-experiment.

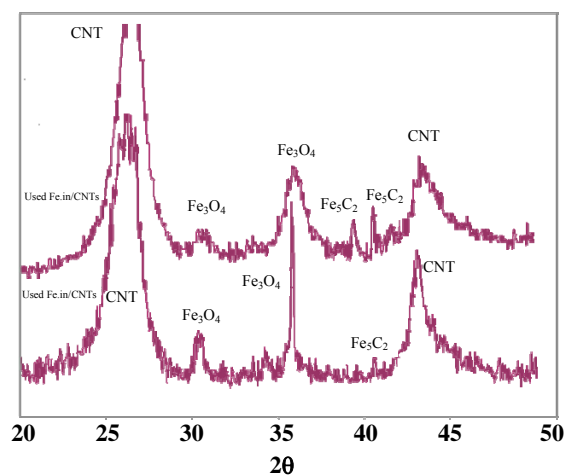


Fig. 12: XRD spectra for the used catalysts

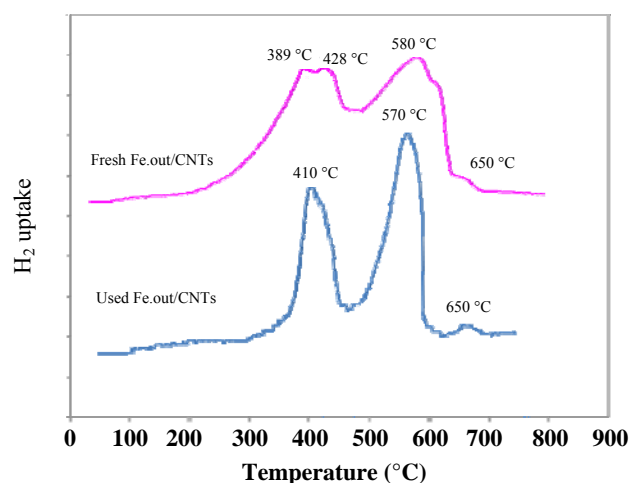


Fig. 13: TPR profiles of the fresh and used Fe.out/CNTs catalysts.

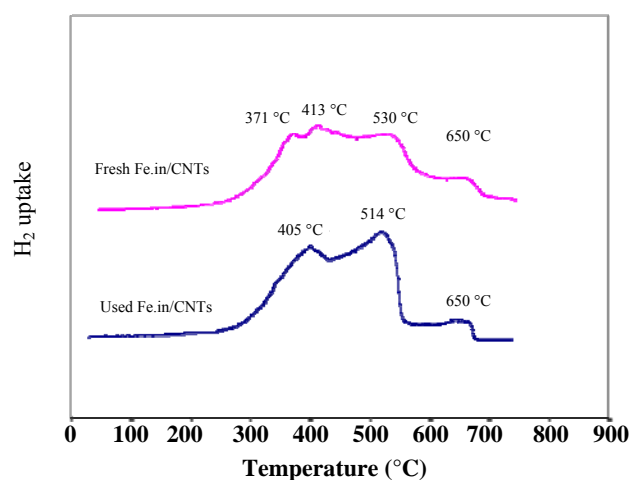


Fig. 14: TPR profiles of the fresh and used Fe.in/CNTs catalysts.

Table 2: The degree of reduction of the fresh and used catalysts.

Catalyst	Degree of reduction (DR _T) (%)
Fresh calcined Fe.out/CNTs	57
Fresh calcined Fe.in/CNTs	71
Used Fe.out/CNTs	33
Used Fe.in/CNTs	52

Fe.in/CNTs catalyst experienced a higher degree of reduction (DR_T=71%) compared to Fe.out/CNTs catalyst (DR_T=57%). Higher degree of reduction will make more iron atoms to be available for FTS reaction in the Fe.in/CNTs catalyst compared to the Fe.out/CNTs catalyst.

Figs. 13 and 14 also show the TRP patterns of the used Fe.out/CNTs and Fe.in/CNTs catalysts. As shown in Figs. 13 and 14, the TPR of the used catalysts could be compared with those of fresh calcined catalysts to see the formation of different phases in the course of FT reaction. Figs. 13 and 14 demonstrate that the following changes have occurred due to the reaction:

1. The first and second peaks in TPR of the fresh calcined catalysts have been transferred to one peak with a temperature close to the second TPR peaks temperature. This peak can be assigned to the reduction of Fe₃O₄ to FeO.

2. The temperature of the third TPR peak is decreased from 580 to 570°C and 530 to 514°C for Fe.out/CNTs and Fe.in/CNTs catalysts, respectively. This peak can be assigned to the reduction of FeO to metallic Fe.

3. The degree of reduction of the Fe.out/CNTs catalyst decreased from 57 to 33% and that of the Fe.in/CNTs catalyst from 71 to 52%.

The decline in the reduction peak temperatures of the used catalysts is due to sintering of the active metal particles. Generally large particles can be reduced easier than the small particles. Sintering of the particles also decreases the degree of reduction of the catalysts. Higher decrease in the degree of reduction in Fe.out/CNTs catalyst is due to higher degree of sintering in this catalyst as also confirmed by TEM analysis.

Fischer-Tropsch Synthesis

The performance of the Fe.in/CNTs and Fe.out/CNTs catalysts in the Fischer-Tropsch synthesis were tested in a fixed bed micro-reactor. All the reactions were performed under a set of standard conditions (275 °C, 2MPa, H₂:CO = 2). Both catalysts reached their highest

activity within 48 h. Afterwards, they showed different stability pattern within a time period of 720 h. Table 3 presents the FT synthesis rate (g CH/g cat./h), %CO conversion and different product selectivities during first 48 hours of FT synthesis (maximum catalytic activity). As shown in Table 3, the FT synthesis productivity of the Fe.in/CNTs catalyst (0.336 g CH/g cat/h) is significantly greater than that of the Fe.out/CNTs catalyst (0.272 g CH/g cat/h). Several reasons can be associated with the improvement in FT synthesis productivity of Fe.in/CNTs catalyst. TEM and XRD results showed that the average size of the particles for Fe.out/CNTs and Fe.in/CNTs catalysts were about 14 and 7 nm, respectively. Lower particle sizes in the case of Fe.in/CNTs catalyst increases the active metal surface area which in turn leads to higher FTS rate. Also, it has been postulated that iron carbides are the active phases for FTS reaction [12]. As discussed earlier, H₂-TPR analysis revealed that the reducibility of the Fe.in/CNTs catalyst was higher compared with the Fe.out/CNTs. This phenomenon can result in the formation of more catalytically active carbide species during FTS. Also the products distribution of Fe.in/CNTs catalyst shows a significant shift to the higher molecular weight hydrocarbons. The data show that CH₄ selectivity of the Fe.in/CNTs catalyst is about 6% lower than that of the Fe.out/CNTs catalyst. Also C₅⁺ selectivity of the Fe.in/CNTs is about 7.6% higher than that of the Fe.out/CNTs. CO₂ selectivities of the Fe.in/CNTs and Fe.out/CNTs catalysts are comparable, indicating similar water-gas shift activity for both catalysts. It seems that, confinement of the reaction intermediates inside the pores in the case of Fe.in/CNTs catalyst can enhance their contact with iron particles, favoring the growth of longer chain hydrocarbons. In addition, the inner sides of the CNTs are electron deficient [14-17] and can enhance the dissociation of CO resulting in production of higher chain hydrocarbons for Fe.in/CNTs catalyst.

It is difficult to compare the productivity data of this research with the catalysts utilized in a reactor that is operated under commercial conditions since the operation conditions are a little different. The commercial reactor working with supported iron catalyst [21] utilized by Sasol is 5 m diameter and 22 m tall. The reactor volume containing catalyst is ~290 m³. The output from the plant is 2500 bbl/day; if one assumes a density of the product of 1 g/cm³, the output is ~16600 kg/h. This corresponds

Table 3: FT synthesis results during first 48 h.

Catalyst	% CO Conversion	FTS rate (g CH/g cat./h)	CO ₂ selectivity	CH ₄ selectivity	C ₂ -C ₄ selectivity	C ₅ + selectivity
Fe.in/ CNTs	85.2	0.336	27.3	19.2	13	40.5
Fe.out/CNTs	69.7	0.272	27.5	25.2	14.4	32.9

to a productivity of ≈ 58 kg/h/m³. The catalyst loading is about 20 wt %, so the productivity would be 0.3 (g of hydrocarbon)/(g of cat)/h. The data presented in Table 3 show that the FT synthesis productivity of the Fe.in/CNTs catalyst (0.336 g CH/g cat/h) and that of the Fe.out/CNTs catalyst (0.272 g CH/g cat/h) are as good as that of the commercial catalyst utilized by Sasol [21].

Fig. 15 presents the %CO conversion changes with the duration of FT synthesis for both catalysts. As it can be seen, for both catalysts, the %CO conversion sharply decreases in the first days, and then levels off. However, the decrease for Fe.out/CNTs catalyst is more significant. For the Fe.in/CNTs catalyst the %CO conversion drops by 26.8% during 720 h FT synthesis while, in the case of Fe.out/CNTs catalyst the decrease in %CO conversion is 46.4%.

The shape of declining curves of both catalysts is similar. The deactivation curve sloped steeply at first and then moderately and finally very slowly. This Figure shows that a plateau region is reached after about 300 h for Fe.in/CNTs catalyst and after 450 h for Fe.out/CNTs catalyst. For both catalysts, the deactivation could be simulated with power law expressions:

$$\text{Fe.in/CNTs: } X_{\text{CO}} = 193.44 T_{(\text{h})}^{-0.1874} \quad (10)$$

$$\text{Fe.out/CNTs: } X_{\text{CO}} = 745.39 T_{(\text{h})}^{-0.482} \quad (11)$$

Assuming the deactivation rate is:

$$-\frac{dX}{dt} = kX^n \quad (12)$$

After integration and data reduction by least square fit, the power order (n) can be determined as 6.4 and 3.1 for the Fe.in/CNTs and the Fe.out/CNTs catalysts respectively. These values are in the range that ordinary metal catalysts would experience during sintering [22]. However the lower power order of 3.1 for the Fe.out/CNTs catalyst demonstrates that the rate of sintering for this catalyst during 720 h FT synthesis was significantly higher than that for the Fe.in/CNTs catalyst. The results of TEM tests showed that the rate of sintering of the particles located on the outer surfaces of the carbon nano tubes (Fe.out/CNTs

catalyst) was higher than that of the particles located on the inner layers of the tubes (Fe.in/CNTs catalyst). Also, the results of XRD tests are shown in Table 1 confirmed the higher cluster growth during 720 h FT synthesis reaction for Fe.out/CNTs catalyst. FT synthesis temperature is too low to boost the cluster growth at the catalyst surface but it seems that water vapor increases the oxidation–reduction cycles on the catalyst surface which in turn leads to cluster growth or sintering. These results verify that to have a carbon nanotubes supported iron catalyst with longer lifetime and higher activity, it is necessary to distribute the active metal particles in the inner layers of the carbon nano tubes. Decreasing the sintering rate of the iron particles which are located on the outer layer of the CNTs by introducing functional groups and defects that can act as anchoring sites for the iron particles, is one of the specific objectives of the ongoing research at our lab.

The uncondensed vapor stream of cold trap was reduced to atmospheric pressure through a pressure letdown valve. The composition of this stream was quantified using an on-line gas chromatograph. The contents in hot and cold traps were removed every 24 h and the hydrocarbon and water fractions separated. The contents of these traps were analyzed using a Varian CP 3400 GC equipped with a Petrocol Tmdh fused silica capillary column and a Flame Ionization Detector (FID) equipped in an offline GC. Fig. 16 display the methane and C₅⁺ liquid hydrocarbon selectivity variations with reaction time for both catalysts. This figure show that for both catalysts, CH₄ selectivity decreases with time-on-stream during 720h FT synthesis at 275°C and 2 MPa. This figure also shows that for both catalysts the C₅⁺ selectivity increases during 720h FT synthesis. The results presented in this figure clearly demonstrate that the used catalysts are more selective to higher molecular weight hydrocarbons than the fresh catalysts. It seems that the steric hindrance for dissociative adsorption of CO and –CH₂– monomer and addition of this monomer to the growing chain is less in the sintered larger cobalt clusters. In the other hand, chain propagation and growth probability on the sintered larger

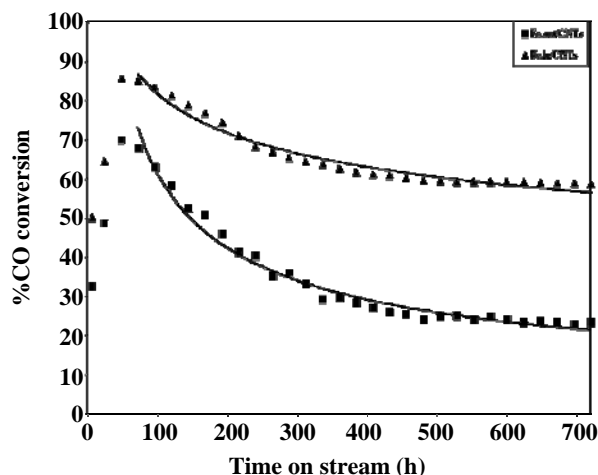


Fig. 15: Changes in %CO conversion with time on-stream for Fe.in/CNTs and Fe.out/CNTs catalysts.

cobalt clusters in the case of used catalysts is more than that of the fresh catalysts. It can be concluded that sintering of the smaller particles leads to enhancement of C_{5+} selectivity and suppression of CH_4 production with time on stream. There is a slight shift toward lighter hydrocarbons (6.3% increases in C_5^+) during the reaction period for the Fe.in/CNTs catalyst.

In contrary, Fe.out/CNTs catalyst experienced an increase of 11.5% in C_5^+ selectivity in the course of 720 h FT synthesis. This could be related to higher drop in CO conversion and the higher increase in particle sizes in the case of Fe.out/CNTs catalyst compared to Fe.in/CNTs catalyst. Higher rate of sintering of the particles located on the outer layers of the tubes increases the ratio of the particles located inside to the particles located on the outside layer of the tubes with increasing time-on-stream. Confinement of the reaction intermediates inside the pores can enhance their contact with iron particles, favoring the growth of longer chain hydrocarbons. In addition, the inner sides of the CNTs are electron deficient and can enhance the dissociation of CO resulting in production of higher chain hydrocarbons. Increasing the ratio of the particles located inside to the particles located on the outside layer of the tubes is believed to be another reason for enhancement of C_{5+} selectivity and suppression of CH_4 .

CONCLUSIONS

The results of this research revealed that the deposition of iron particles inside the carbon nano tubes pores improves the activity, selectivity and lifetime of the carbon nanotubes supported iron catalyst, most likely due to difference in

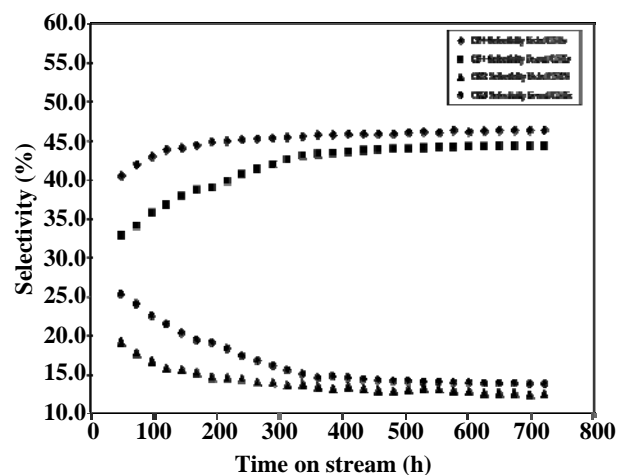


Fig. 16: Changes in C_5^+ and CH_4 selectivities with time on-stream for Fe.in/CNTs and Fe.out/CNTs catalysts.

electronic properties of the inner and outer surface of the CNTs, and confinement effects. The inner sides of the CNTs are electron deficient and can enhance reducibility and the dissociation of CO, resulting in higher specific activity for the metal particles located in the inside layer of the tubes. Confinement of reaction intermediates inside the channels increases the contact time with active metal sites, resulting in production of heavier hydrocarbons. Sintering is the main source of irreversible deactivation in the CNTs supported iron FT synthesis catalysts. Due to the electron deficiency of the inner sides of the CNTs, the interaction between the iron and the support is stronger leading to lower rates of sintering as compared with the particles located on the outer layers of the CNTs.

Nomenclature

P	Pressure, MPa
T	Temperature, °C
S	Selectivity, %
n_{cl}	Number of nanotubes with close-cap per mass unit
n_{op}	Number of nanotubes with open-cap per mass unit
d_{in}	Inner diameter of CNTs
d_{out}	Outer diameter of CNTs
L	Average length of CNTs
A	Surface area, area/mass unit
%CO	Percent of CO conversion, mol%
X	Conversion

Abbreviations

FTS	Fischer-Tropsch Synthesis
WGS	Water-gas shift

CNTs	Carbon nanotubes
XRD	X-ray diffraction
TPR	Temperature programmed reduction
GC	Gas chromatograph
ICP	Inductively coupled plasma
TEM	Transition electron microscopy
BET	Brunauer, Emmett, and Teller

Received : Dec. 30, 2009 ; Accepted : Mar. 15, 2010

REFERENCES

- [1] Anderson R.B., "The Fischer-Tropsch Synthesis", Orlando, FL: Academic Press, (1984).
- [2] Dry M.E., The Fischer-Tropsch Synthesis, *Catal. Sci. and Tech.*, **1**, p. 159 (1981).
- [3] Bartholomew C.H., New Trends in CO Activation, *Stud. in Surf. Sci. and Catal.*, **64**, p. 158 (1991).
- [4] Bukur D.B., Lang X., Mukesh D., Zimmerman W.H., Rosynek M.P., Li C., Development of Improved Fischer-Tropsch Catalyst, *Ind. Eng. Chem. Res.*, **29**, p. 1588 (1990).
- [5] Malek Abbaslou R.M., Tavasoli A., Dalai A.K., Iron Catalysts Supported on Carbon Nanotubes for Fischer-Tropsch Synthesis Effect of Catalytic Site Position, *Appl. Catal. A: Gen.*, **367**, p. 47 (2009).
- [6] Tavasoli A., Sadaghiani K., Khorashe F., Seifkordi A.A., Rohani A.A., Nakhaeipour A., Cobalt Supported on Carbon Nanotubes-A Promising Novel Fischer-Tropsch Synthesis Catalyst, *Fuel Proc. Technol.*, **89**, p. 491 (2007).
- [7] Tavasoli A., Rashidi A.M., Sadaghiani K., Karimi A., Khodadadi A., Mortazavi Y., "Carbon Nanotubes Supported Cobalt Catalyst for Converting Synthesis Gas Into Hydrocarbons", European Patent EP1782885 (2005).
- [8] Tavasoli A., Sadaghiani K., Nakhaeipour A., Ghalbi Ahangari M., Cobalt Loading Effects on the Structure and Activity for Fischer-Tropsch and Water-Gas Shift Reaction of Co/Al₂O₃ Catalysts, *Iran. J. Chem. Chem. Eng.*, **26**, p. 9 (2007).
- [9] Ma W., Kugler E.L., Wright J., Dadyburjor D.B., Mo-Fe Catalysts Supported on Activated Carbon for Synthesis of Liquid Fuels by the Fischer-Tropsch Process: Effect of Mo Addition on Reducibility, Activity and Hydrocarbon Selectivity, *Energy Fuels*, **20**, p. 2299 (2006).
- [10] Guczi L., Stefler G., Geszti O., Koppány Zs., Kónya Z., Molnár É., Urbánc M., Kiricsi I., CO Hydrogenation over Cobalt and Iron Catalysts Support over Multi wall Carbon Nanotubes: Effect of Preparation, *J. Catal.*, **244**, p. 24 (2006).
- [11] Bahome M.C., Jewell L.L., Padayachy K., Hildebrandt D., Glasser D., Datye A. K., Coville N. J., Fe-Ru Small Particle Bimetallic Catalysts Supported on Carbon Nanotubes for Use in Fischer-Tropsch Synthesis, *Appl. Catal. A: Gen.*, **328**, p. 243 (2007).
- [12] Van Steen E., Prinsloo F.F., Some Evidence Refuting the Alkenyl Mechanism for Chain Growth in Iron-Based Fischer-Tropsch Synthesis, *Catal. Tod.*, **71**, p. 327 (2002).
- [13] Bahome M.C., Jewell L.L., Hildebrandt D., Glasser D., Coville N. J., Fischer-Tropsch Synthesis over Iron Catalysts Supported on Carbon Nanotubes, *Appl. Catal. A: Gen.*, **287**, p. 60 (2005).
- [14] Chen W., Pan X., Bao X., Tuning of Redox Properties of Iron and Iron Oxides via Encapsulation within Carbon Nanotubes, *Chem. Soc.*, **129**, p. 7421 (2007).
- [15] Pan X., Fan Z., Chen W., Ding Y., Luo H., Bao A.N.D.X., Enhanced Ethanol Production Inside Carbon-Nanotube Reactors Containing Catalytic Particles, *Nature*, **6**, p. 507 (2007).
- [16] Menon M., Andriotis A.N., Froudakis G.E., Curvature Dependence of the Metal Catalyst Atom Interaction with Carbon Nanotubes Walls, *Phys. Lett.*, **320**, p. 425 (2000).
- [17] Santiso E.E., Adsorption and Catalysis: The Effect of Confinement on Chemical Reaction, *Appl. Surf. Sci.*, **252**, p. 766 (2005).
- [18] Granqvist C.G., Buhrman R.A., Sintering Behavior of Nickel Particles Supported on Alumina Model Catalyst in Hydrogen Atmosphere, *J. Catal.*, **42**, p. 477 (1976).
- [19] Sehested J., Carlsson A., Janssens T.V.W., Hansen P.L., Datye A.K., Sintering of Nickel Steam-Reforming Catalysts on MgAl₂O₄ Spinel Supports, *J. Catal.*, **197**, p. 200 (2001).
- [20] Joo S.H., Choi S.J., Oh I., Kwak J., Liu Z., Terasaki O., Ryoo R., Ordered Nanoporous Arrays of Carbon Supporting High Dispersions of Platinum Nanoparticles, *Nature*, **412**, p. 169 (2001).
- [21] Davis B. H., Fischer-Tropsch Synthesis: Comparison of Performances of Iron and Cobalt Catalysts, *Ind. Eng. Chem. Res.*, **46**, p. 8938 (2007).
- [22] Bartholomew C.H., Mechanisms of Catalyst Deactivation, *Appl. Catal. A: Gen.*, **212**, p. 17 (2001).